JOURNAL OF SOLID STATE CHEMISTRY 89, 94–105 (1990)

On the Peritectic Transformation in $Bi_4Sr_3Ca_3Cu_4O_{16+x}$ and Its Role in the Formation of the $Bi_2Sr_2Ca_2Cu_3O_{10}$ Phase

J. S. LUO, F. FAUDOT, J.-P. CHEVALIER, R. PORTIER, AND D. MICHEL

C.E.C.M-C.N.R.S., 15, rue G. Urbain, 94407 Vitry Cédex, France

Received February 6, 1990; in revised form June 15, 1990

We have studied the structural and microstructural changes of $Bi_4Sr_3Ca_3Cu_4O_{16+x}$ on annealing close to its melting point and correlated these with the thermal stability and the electrical properties. Thermal analyses suggest that the $Bi_4Sr_3Ca_3Cu_4O_{16+x}$ phase undergoes a peritectic or peritectic-like transformation, accompanied by oxygen loss, just before complete melting. This transformation leads to the formation of the $Bi_2Sr_2Ca_2Cu_3O_{10}$ phase as identified by X-ray diffraction (XRD) and confirmed by electrical resistivity measurements. Electron microscopy shows that $Bi_4Sr_3Ca_3Cu_4O_{16+x}$ samples maintain their lamellar morphology after transformation and are locally decomposed into a majority $Bi_2Sr_2Ca_2Cu_3O_{10}$ phase bounded by an amorphous phase. A thin layer of $Bi_4Sr_3Ca_3Cu_4O_{16+x}$ phase is systematically observed between this amorphous phase and the transformed regions. In the latter, a stacking sequence corresponding to a Bi–Sr–Ca–Cu–O phase with a structure based on four Cu–O layers is also observed. Finally, we discuss the consequences of this transformation on electrical properties and on the conditions required for the preparation of a pure $Bi_2Sr_2Ca_2Cu_3O_{10}$ phase.

Introduction

After the observation of superconductivity in the rare earth-free Bi–Sr–Cu–O system with $T_c \sim 20$ K by Michel *et al.* (*1*), the addition of calcium has led to the discovery of bulk superconductivity at 85 K and evidence for a superconducting transition near 110 K in the Bi–Sr–Ca–Cu–O system (*2, 3*). In the $Bi_2Sr_2Ca_{n-1}Cu_nO_{2n+4}$ structural family, as well as in the homologous thallium family, T_c increases with the number of Cu–O layers when n varies from 1 to 3 (*4–14*). For $n = 1$ and $n = 2$, the structures of various Bi–Sr–Ca–Cu–O phases have been determined from single crystals (*10, 15*) and pure phases have been successfully prepared by solid state reaction as well as by other methods (*10–12, 16–18*). It seems much more difficult to synthesize a single phase for $n = 3$, corresponding to the highest value of $T_c = 110$ K (hereafter compositions will be denoted by their cation stoichiometry, e.g., 2223 for $Bi_2Sr_2Ca_2Cu_3O_{10}$). This latter is generally only found in intergrowth with 2201 and 2212 phases as shown by transmission electron microscopy (TEM) observations (*12, 19*), and very critical temperature control is required to form the 2223 phase. Tarascon *et al.* (*10, 20*) report that heating single phase 4334 (4334 having the same structure as 2212 due to the possible substitution of Ca on Sr sites) which initially has $T_c = 85$ K, near its melting point, produces a sharp resistivity drop at 110 K. Huang *et al.* (*21*) obtain a majority 2212 phase even with a 2223 starting composition by sintering in air at 850°C. In this case, no 2223

0022-4596/90 $3.00

phase is obtained, and superconductivity near 110 K (indicative of the 2223 phase) is only observed for samples heated at 880°C for a few days. These results suggest that the formation of the 2223 phase must be closely related with the melting characteristics of the 2212 phase. This melting behavior is complex, since two endothermic peaks, at ~870°C and ~910°C, are observed by differential thermal analysis (DTA) and, using thermogravimetry (TG), the reaction at ~870°C is found to be accompanied by a weight loss (*10, 21, 22*).

The mechanisms and phase relations for this transformation are still not fully understood, and the equilibrium phase diagram is not completely known, either. From powder X-ray diffraction data, together with electrical resistivity measurements, Pekker *et al.* (*23*) propose that 2201 and 2212 are equilibrium phases at room temperature. 2223 would be stable above around 880°C, and only metastable at room temperature. High temperature X-ray diffraction indicates that the 2212 phase disappears above 870°C whereas the 2223 phase seems to remain stable up to 890°C (*24*). Recently, several mechanisms have been proposed for the formation of the 2223 phase, such as the dissociation reaction of the 2212 phase into the 2223 and 2201 phases (*25*) or the precipitation of the 2223 phase from a partially melted liquid (*26*). However, few studies have treated the microstructural aspects of the transformation. Up to now, the 2223 phase has essentially only been obtained in a nearly pure form with substitution of lead (*27–29*). The effect of this substitution is not well understood. It may accelerate the kinetics of the phase formation and/or extend the domain of phase stability.

Here, we present a microstructural investigation of the phase transformation behavior of 2212-type phase with 4334 composition, in combination with thermal analysis, X-ray diffraction (XRD), and electrical resistivity measurements. First, we demonstrate that the 4334 phase undergoes a peritectic transformation before complete melting. We then show that the 2223 phase is the main product of this transformation and that the stability domain of the 2223 phase is likely to be rather limited. In the third part, we report observations both by scanning electron microscopy (SEM) and by transmission electron microscopy (TEM). These show that the 2223 phase still has a characteristic plate-like morphology and is formed by intergrowth within the host 4334 phase. We also show evidence for a four Cu–O sheet structure with 2.2-nm blocks in the 2223-rich regions. Finally, we discuss the possible formation mechanism of the 2223 phase and the relations between this transformation and the conditions for the preparation of pure 2223 phase, as well as the resulting electrical properties.

Experimental Procedure

Ceramic samples are prepared by mixing pure (99.95%) bismuth oxide, calcium carbonate, and copper oxide in proportions corresponding to the $Bi_4Sr_3Ca_3Cu_4$ composition. Powders are thoroughly mixed, calcinated at 800°C in air for 16 hr, and furnace cooled. They are reground and pressed into bars of size 3 × 5 × 20 mm which are subsequently sintered at 850°C in air for 150 hr and then furnace cooled to room temperature. Several intermediate grindings are carried out to ensure good homogeneity. A platinum foil is employed to prevent possible contamination of the samples from the alumina crucibles.

Differential thermal analysis (DTA) is carried out under a static air atmosphere with a SETARAM M4 apparatus equipped with platinel thermocouple (emf ≈40 μV °C^{-1} at 1000°C). The thermometric and calorimetric apparatus are calibrated with the help of standard substances (*30*) as described by Faudot *et al.* (*31*). Two heating rates (20°C.min^{-1} and 2°C.min^{-1}) are used in or-

der to ascertain their influence on the transformation temperature. About 30 mg of the sintered 4334 phase is ground and hand-pressed into a 25-mm^3 alumina crucible for the DTA experiment. The transformation temperature is conventionally defined as the temperature corresponding to the intersection point between the extrapolated base line on the high temperature side and the tangent at the inflection point on the low temperature side (*32*). Thermogravimetric (TG) experiments are performed under a static air atmosphere using a "MARK 2A" microthermobalance from C.I. Electronics Limited. The apparatus is equally weight calibrated by using pieces of pure platinum. A cylinder (2.5 mm in diameter, 3 mm long) cut from the sintered 4334 bar is used as TG sample. The heating rate is 2°C.min^{-1} and TG sensibility is about 0.45 mg.cm^{-1}.

XRD spectra (filtered Co$K\alpha$ radiation) are recorded using a Philips diffractometer. Lattice parameters are refined by means of a least-squares program. The resulting superconducting oxide is examined on its fracture surface by scanning electron microscopy on a ZEISS DSM950. Transmission electron microscopy is carried out on a JEOL 2000FX analytical and a JEOL 200CX high resolution microscopes. Specimens are prepared from slices by mechanical polishing to ~50 μm thickness followed by argon ion milling at 6 kV with a total gun current (both guns) of 1 mA.

Resistivity measurements are carried out on bars (approximately 2 × 2 × 10 mm) cut from as-sintered samples. A standard four-probe dc method is used with silver paint contacts. The measurement current is 10 mA. In the superconduction state, the maximum detected potential difference is smaller than 1 μV and does not change in sign when the current is reversed.

Results and Discussion

XRD shows that samples sintered at 850°C consist of a single 4334 phase and that the major Bragg peaks can be indexed on the basis of the tetragonal subcell (a = 0.3812 nm, c = 3.058 nm), with some of the weak lines on the basis of a $\sqrt{2}a$ supercell (see Fig. 1a). This result is very similar to that obtained by Tarascon *et al.* (*10*). The DTA curve for this single phase (see Fig. 2a) shows that two peaks, associated with the melting of this single phase, are observed at the heating rate of 20°C.min^{-1}, in agreement with several other authors (*10, 13, 21*). This is consistent with the behavior expected for a compound with noncongruent melting. We observe partial melting of the sample when maintained at the temperature between these two peaks, suggesting that the first endothermic peak is due to a peritectic or peritectic-like transformation of the 4334 phase. Thus the temperature, at which the 4334 phase is decomposed under these experimental conditions (static air, heating rate of 20°C.min^{-1}), is determined to be 871 ± 5°C.

In fact, results obtained in changing experimental conditions reveal that the melting behavior of the 4334 phase is more complicated and that the starting point of the peritectic transformation is very sensitive to parameters such as atmosphere, heating rate, and even gas flow. Figure 2b shows the DTA curve obtained at a much slower heating rate (2°C.min^{-1}) under a static air atmosphere. The first peak, previously observed as a single peak at a heating rate of 20°C.min^{-1}, is now split into three small peaks, suggesting that several reaction probably occur at this stage, i.e., before complete melting. In this case, the initial transformation temperature of the 4334 phase is shifted to 863 ± 5°C, as determined from the first peak. This difference can be explained by kinetic factors for this transformation. For the second and third peaks, we can only estimate the temperatures (bottom points of peak) of the completion of the corresponding transformations. Without deconvolution, they are extrapolated to be at

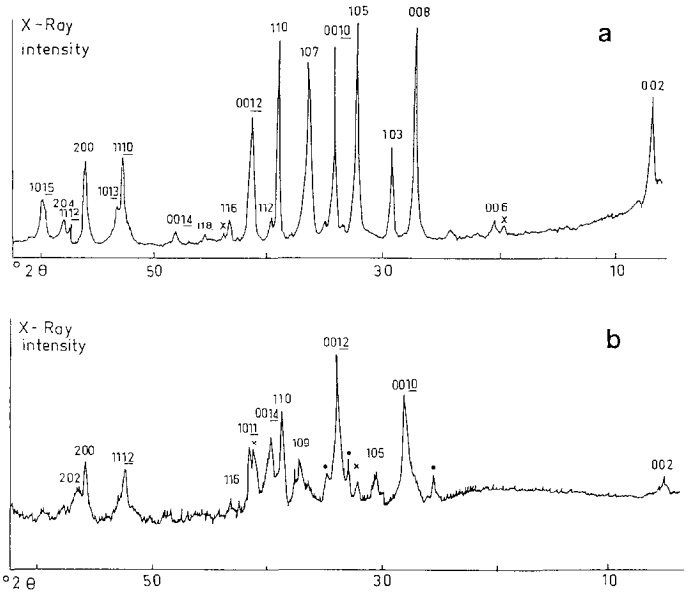

FIG. 1. X-ray diffraction powder spectra (Co$K\alpha$). (a) 4334 sample sintered at 850°C (indexation with a 2212 tetragonal subcell a = 0.3812 nm, c = 3.058 nm. x indicates lines which can be indexed with a unit cell of a = 0.5391 nm and c = 3.058 nm. (b) After annealing at 870°C (indexation with a 2223 tetragonal subcell a = 0.3817 nm, c = 3.700 nm). x indicates the 4334 lines and ● some lines which are not readily indexed.

~873 and ~877°C, respectively. This means that the transformation of the 4334 phase occurs not only in several steps but that the domains of stability for each resulting compound are also very narrow. Figure 2c shows the TG curve for the 4334 phase recorded with the same experimental conditions as for Fig. 2b. Below the peritectic transition temperature a weight change is first observed for single 4334 phase. Considering that the loss or gain of one atom oxygen per unit formula results in a ~1% weight change, the observed effect is an increase of about 0.5 oxygen per unit formula in the range 500–600°C. Thus the stoichiometry of this phase can be changed by annealing at these intermediate temperatures. At higher temperatures, a weight loss occurs and the initial composition is restored at 750°C. A sharp effect is observed at 861°C which, within experimental error, is the starting point of the peritectic reaction determined by DTA under the same conditions. The transformation of the 4334 phase is thus associated with a significant weight loss (most probably a loss of oxygen). This can strongly influence the oxygen partial pressure around the sample. In particular, for a crucible volume of 25 mm^3 in our DTA experiment, the release of ~1% oxygen from an ~30-mg sample would increase the oxygen concentration by ~150 times. This may account for the strong dependence of the transformation temperature on the experimental conditions.

In order to investigate the mechanism of this complex transformation of the 4334 phase, the as-sintered superconductor is annealed at 870°C in air for ~60 hr and then furnace-cooled. The XRD spectrum of the annealed sample can be essentially indexed on the basis of a tetragonal unit cell with a =

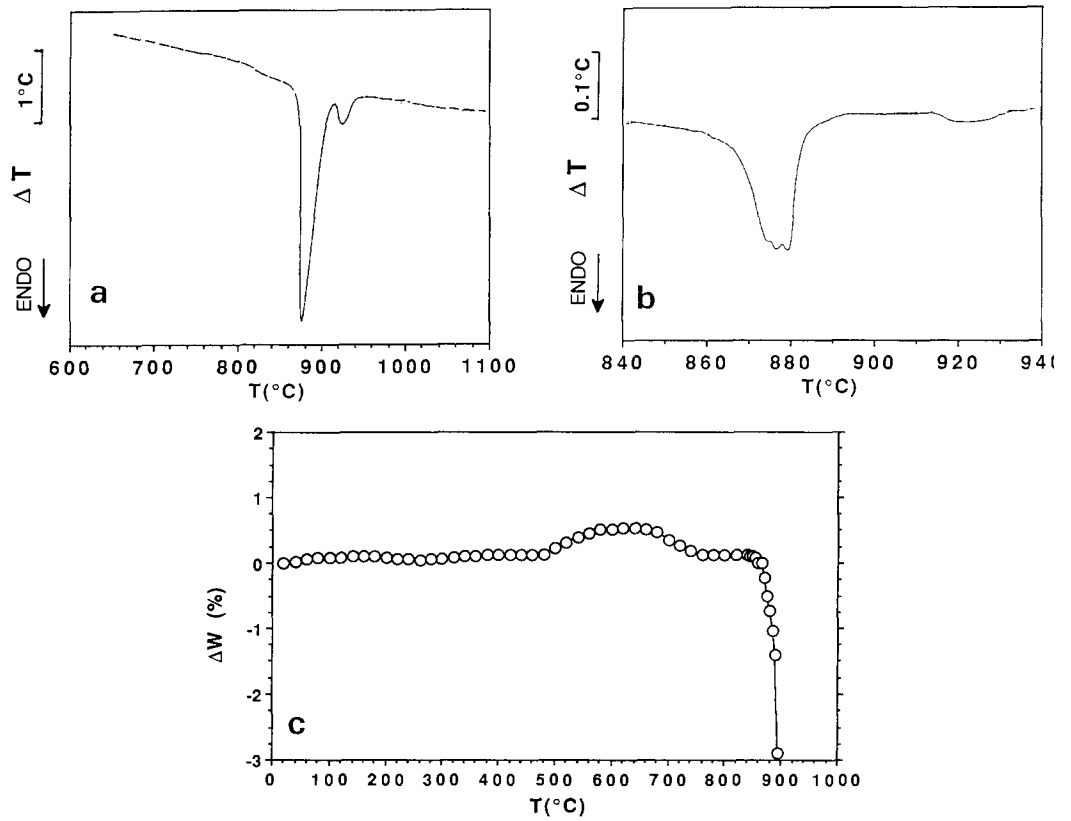

FIG. 2. Thermal analysis results for the 4334 phase: (a) DTA curve obtained at a heating rate of 20°C min^{-1}: the first peak corresponds to the phase stability limit, the transformation temperature is determined to be 871°C using the tangent convention. (b) DTA curve obtained at a heating rate of 2°C min^{-1}, the first peak is split up into three small peaks, indicating a complex melting behavior. The 4334 phase becomes unstable at 863°C. (c) TG curve obtained at a heating rate of 2°C min^{-1}, note the small weight change before melting and the large weight loss after 861°C.

0.3817 nm and c = 3.700 nm, i.e., with the 2223 structure (Fig. 1b). However, the diffraction peaks for the 2223 phase are broad, notable for {001} peaks are present but their intensities remain relatively weak (Fig. 1b). A small fraction of 4334 phase is found, but some lines are unidentified. We therefore propose that the 4334 phase transforms at temperatures in the range ~865–870°C in the following general manner:

$$4334(\text{solid}) \rightarrow \text{liquid} + 2223(\text{solid}) + O_2.$$

Here, the proportion of the liquid phase is limited since the composition differences between the 4334 phase and the 2223 phase are small. This is in agreement with experimental observations. Some other transitory phases may also exist and these may account for some unidentified weak lines in XRD (Fig. 1b). This reaction corresponds to the initial decomposition of the 4334 phase, i.e., to the first endothermic peak observed by DTA. It should be noted that the stability domain of the 2223 phase is therefore only about 10°C, since the two successive reaction occur at ~873 and ~877°C, respectively

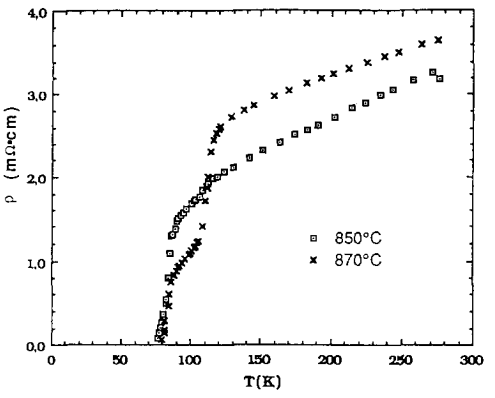

FIG. 3. Comparison of the temperature dependence of electrical resistivity for the 4334 phase before (⊡) and after (x) the transformation.

(Fig. 2b), explaining why the conditions for preparation of the 2223 phase are so critical.

Electrical resistivity measurements confirm the presence of the 2223 phase (see Fig. 3). A sharp drop in resistivity occurs at ~110 K, but zero resistivity is only reached at ~80 K. It should also be noted that, for the nonsuperconducting state, the resistivity of the sample annealed at 870°C is higher than that for the sample annealed at 850°C. This higher resistivity could arise from the contribution of extra, insulating or semiconducting phases formed in the sample after the peritectic transformation.

SEM observation have been made before and after the transformation (see Figs. 4a and 4b). The observation of fracture surfaces reveal that the plate-like morphology, which is characteristic of the 4334 phase, is maintained after the transformation. The surfaces of the platelets, for the sample annealed at 870°C, become rougher and are slightly curved. After transformation, the layered crystals seem to have coalesced and grown along the direction perpendicular to platelets leading to an increase in thickness. There is no evidence for the appearance of a different morphology due to the new phases.

TEM examination of the pure 4334 phase (Fig.5a) reveals that crystals frequently grow in fan-like clusters of thin plates separated by low angle grain boundaries perpendicular to the c axis. The spacing of the c planes is relatively uniform and the corresponding electron diffraction leads to a half c parameter of ~1.53 nm. Some defects are present in the stacking sequence as it is usually observed in layered structures with a large stacking period. Even for a stoichiometric composition, corresponding to a phase of sequence n, some blocks of phase $n - 1$ and $n + 1$ are observed in intergrowth (*33*).

After transformation, the previous regular c spacing, inside grains, is replaced by the coexistence of different c spacings (i.e., intergrowth of different phases), and an amorphous phase is generally observed at the periphery of the transformed regions (Fig. 5b). The diffraction pattern (inset in Fig. 5b) shows that mainly two spacings of ~1.85 and ~1.53 nm in the c direction (half the 2223 and 4334 c parameters, respectively) intergrow. The reflections from the 1.85-nm phase are much more intense, indicating that the majority phase is the 2223 phase. This is in agreement with the XRD data (see Fig. 1b).

High resolution imaging confirms that a spacing of 1.85 nm (2223) is the major constituent in the center of transformed regions. In addition, it is interesting to note the presence of some ~2.2-nm layers in such a majority 2223 phase region and some spacings of 1.53 nm (2212) are also found in intergrowth (Fig. 6). Since the structures of 2212 and 2223 are known, the stacking sequences can be interpreted directly from the images. The dark rows with constant thickness can be assigned to the double Bi–O and Sr–O layers, and these layers are separated by perovskite-like blocks with variable thickness depending on n. Within these blocks the one, two, or three bright fringes correspond to the CuO_2 layers. Our observations of the spacing of ~2.2 nm indicates that it is

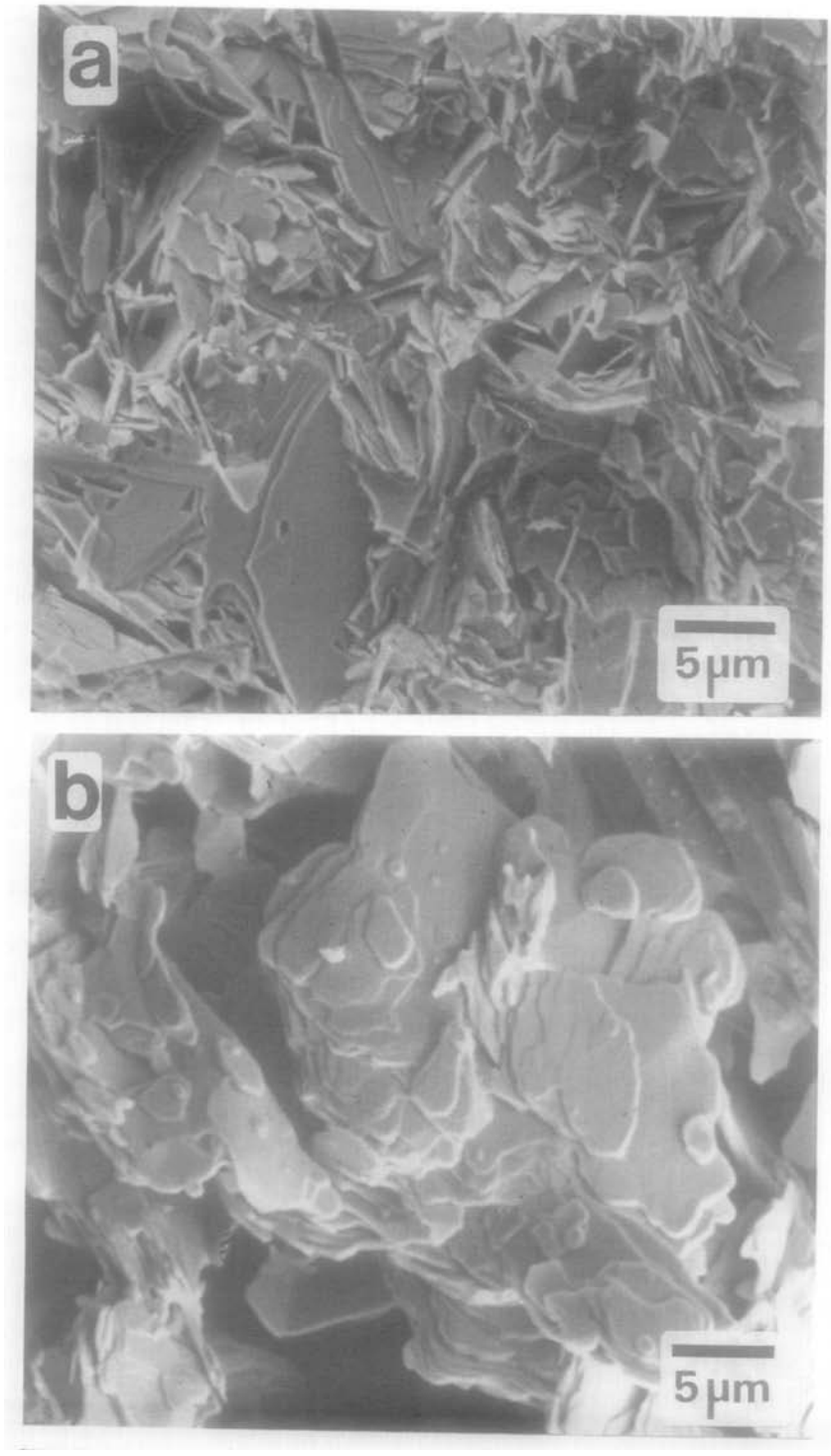

FIG. 4. SEM (secondary electron mode) images. (a) Single 4334 phase obtained at 850°C. (b) After decomposition through annealing at 870°C.

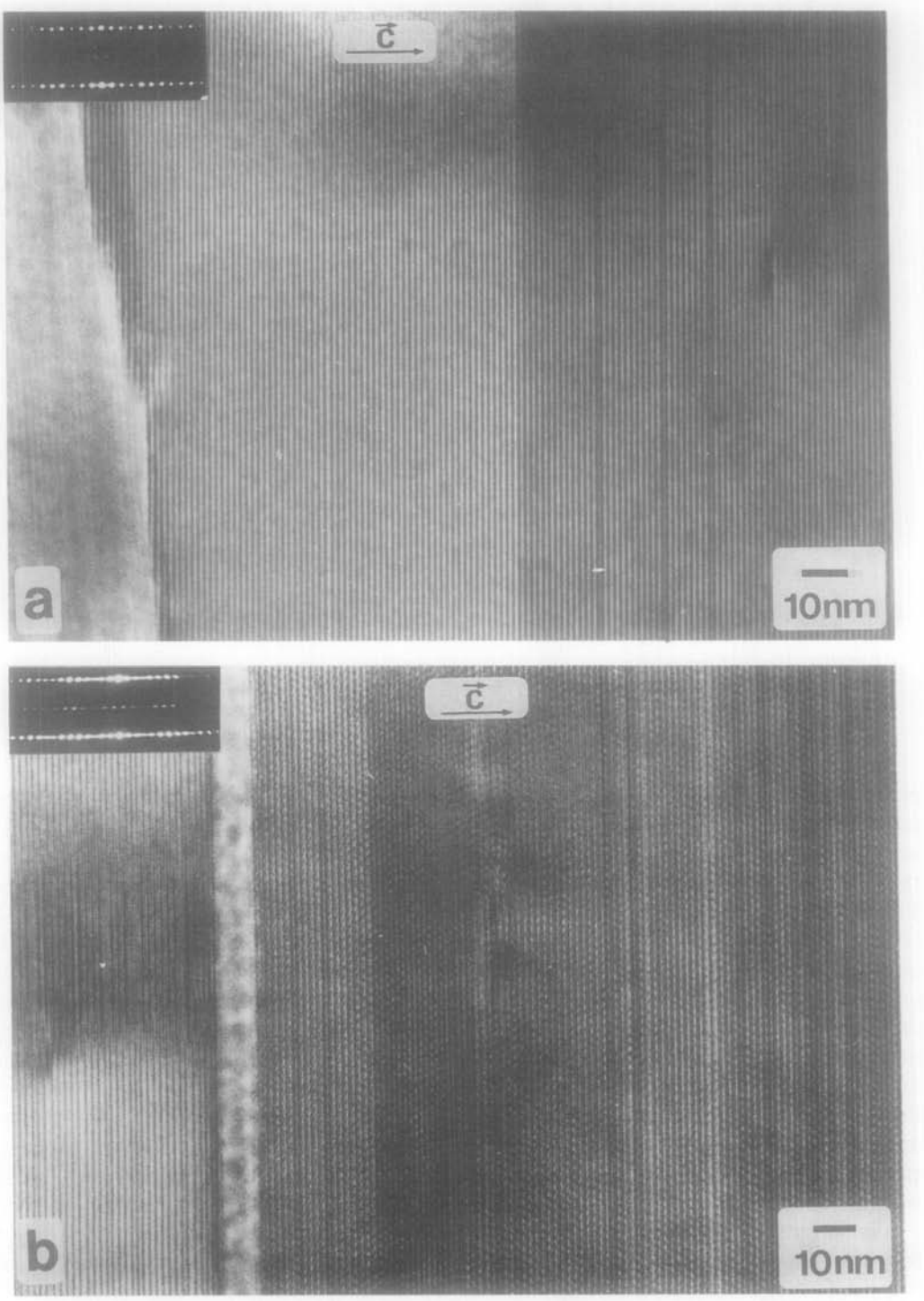

FIG. 5. High resolution transmission electron microscopy (HRTEM) images of a 4334 sample before (a) and after (b) transformation.

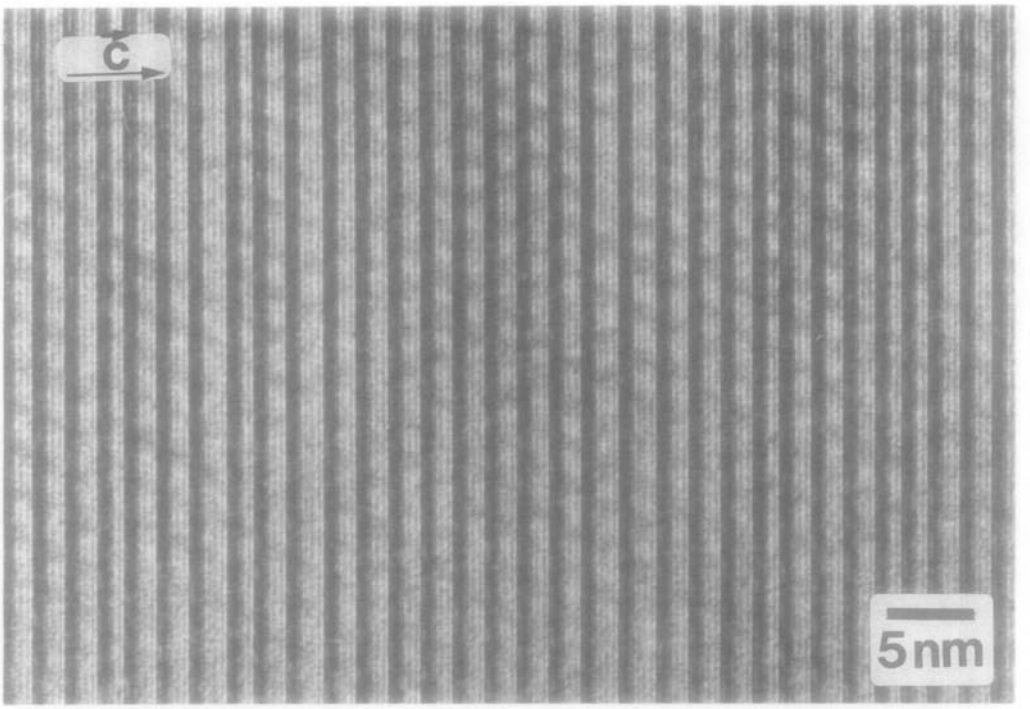

FIG. 6. HRTEM image after transformation of a region inside a grain. The c spacing is mainly ~1.85 nm (2223), but some 1.53-nm (4334) and 2.2-nm (2234) spacings are also observed.

possible to locally observe a 2234 structure of four CuO_2 layers with a half c parameter of ~2.2 nm. This 2234 phase is similar to that obtained by Hervieu *et al.* (*34*) in the Tl–Ba–Ca–Cu–O system and by Rao *et al.* (*35*) on Pb-substituted Bi–Sr–Ca–Cu–O compound. In the latter compound, Werder *et al.* (*36*) observed, by TEM, the existence of this phase with a c axis parameter of 4.32 nm in grains containing no intergrowth defects. In our case, we are not able to define the stability domain of 2234 but the existence of this phase will obviously complicate the phase diagram in the temperature region considered.

Figure 7 shows details of the spatial distribution of the stacking sequences near the periphery of the transformed region. Here, the c spacing is regular and corresponds to the 4334 phase, while intergrown blocks with different c spacings are observed inside the grain. These regions of 4334 spacings are systematically observed at the boundaries and are only of order 10 nm thick in general. Ramesh *et al.* (*37, 38*) also observe a shell of 4334 around a dominant 2223 phase and propose that this may explain the two-step superconducting transition generally observed in polycrystalline sample.

If we consider the consequences of the proposed peritectic transformation, for a starting composition of 4334, the formation of the 2223 phase must proceed via a diffusion of cations in order to obtain the appropriate composition. In this case, some Ca and Cu atoms have to diffuse in the opposite direction to that of Sr and Bi atoms since the 2223 phase differs in one layer of $CaCuO_2$ from the 4334 parent phase. Conse-

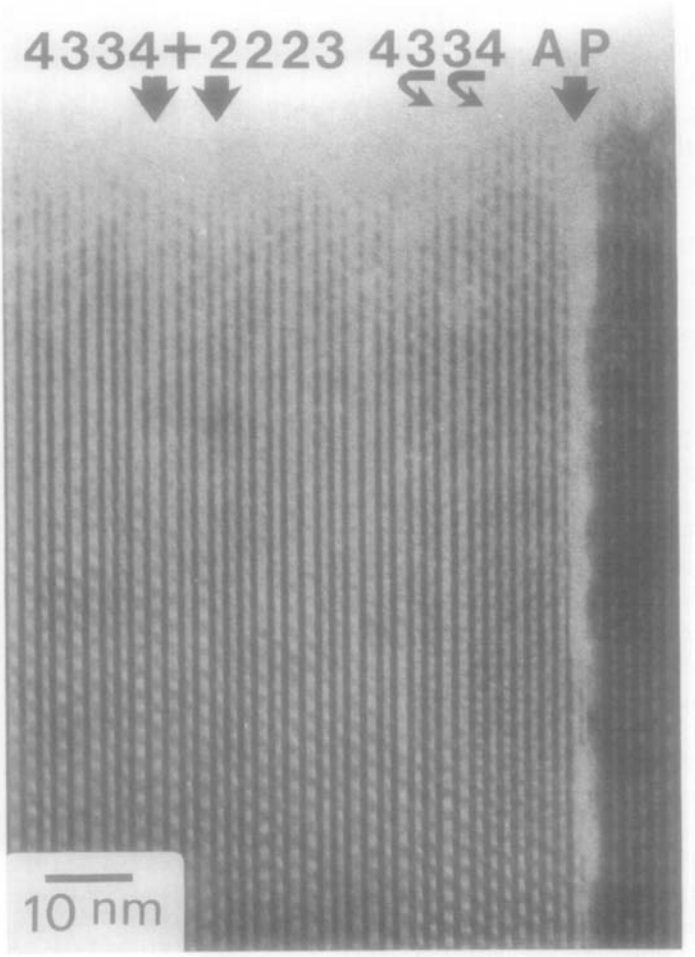

FIG. 7. HRTEM image after transformation showing the presence of 4334 + 2223 spacings inside the grain, a layer of 4334 spacing close to the boundary, and an amorphous phase (AP) at the boundary.

quently, the liquid phase produced is Ca and Cu poor and Bi enriched. Upon cooling below the transformation temperature, this liquid phase will solidfy to form first a layer of 4334 phase around regions of majority 2223 phase and then the amorphous phase, which is likely to be the last remnant of the liquid phase.

The possible effects of this transformation and the induced microstructure will be then clearly deleterious on the electrical properties. The coexistence of both intergrowths of 4334 and 2234 within a majority 2223 phase and a "shell" of 4334 phase around the transformed regions will lead to a broad and stepped superconducting transition. In addition, the amorphous phase separating the regions of superconducting phase is likely to limit the critical current density.

Conclusion

We have investigated the behavior of the 4334 single phase near its noncongruent melting point. DTA and TG results show

that partial melting begins at ~863°C in air and is associated with an oxygen loss. The 4334 phase thus undergoes a peritectic or peritectic-like reaction and is mainly transformed into the 2223 phase at this stage, conserving its characteristic plate-like morphology.

After the transformation we observe regions essentially transformed to the 2223 phase, bounded by an amorphous phase. A thin layer of 4334 is systematically observed between 2223 and the amorphous phase. c spacings of ~2.2 nm are observed, corresponding to a 2234 structure with four Cu–O layers, in regions which are essentially of 2223 phase. This composite microstructure, with the coexistence of 4334, 2234, and 2223 intergrown, on such a fine scale, may explain the broad superconducting transition despite the presence of a majority, but nevertheless imperfect, 2223 phase.

The conditions for the preparation of the 2223 phase will therefore be very critical, because of the long range diffusion needed, the locally nonequilibrated oxygen partial pressure, and especially its narrow temperature stability domain. In fact, we have only been able to prepare a well-crystallized majority 2223 phase using rapidly quenched alloy precursors (*39*). Here, we believe that the use of these metallic precursors accelerates the kinetics of the reaction and we estimate that we obtain more than 80% of the 2223 phase, starting from an alloy of composition 2223.

For conventionally processed material, it is quite clear that it will not be possible to prepare a 2223 superconducting phase with good properties starting from the peritectic decomposition of the 4334 phase. This is difficult to avoid since this phase is the stable majority phase at room temperature, even for the 2223 composition. The presence of an amorphous phase with an adjoining layer of 4334 phase will give poor values of critical currents and a broad superconducting transition.

Acknowledgments

The authors thank Drs. M. Harmelin, Y. Calvayrac, and O. Dimitrov for valuable comments and suggestions. We are also grateful to the CNRS (ARC "Microstructure des Nouveaux Supraconducteurs") for financial support.

References

1. C. Michel, M. Hervieu, M. M. Borel, A. Grandin, F. Deslandes, J. Provost, and B. Raveau, *Z. Phys., B* **68,** 421 (1987).
2. M. Maeda, Y. Tanaka, M. Fukutomi, and T. Asano, *Japan J. Appl. Phys. Lett.* **27,** L209 (1988).
3. C. W. Chu, J. Bechtold, L. Gao, P. H. Hor, Z. J. Huang, R. L. Meng, Y. Y. Sun, Y. Q. Wang, and Y. Y. Xue, *Phys. Rev. Lett.* **60,** 941 (1988).
4. Z. Z. Sheng and A. M. Herman, *Nature (London)* **332,** 55 (1988).
5. Z. Z. Sheng, A. M. Herman, A. el Ali, C. Almasan, J. Estrada, T. Datta, and R. J. Matson, *Phys. Rev. Lett.* **60,** 937 (1988).
6. R. M. Hazen, L. N. Finger, R. J. Angel, C. T. Prewitt, N. L. Ross, C. G. Hadidacos, P. J. Heaney, P. R. Verlen, Z. Sheng, A. el Ali, and H. Hermann, *Phys. Rev. Lett.* **60,** 1657 (1988).
7. S. Parkin, V. Y. Lee, E. M. Engler, A. I. Nazzal, T. C. Huang, G. Gorman, R. Savoy, and R. Beyers, *Phys. Rev. Lett.* **60,** 2539 (1988).
8. C. Politis, and H. Luo, *Mod. Phys. Lett. B* **2,** 793 (1988).
9. J. Akimitsu, A. Yamazaki, H. Sawa, and H. Fujiki, *J. Appl. Phys. Lett.* **27,** L2080 (1988).
10. J. M. Tarascon, Y. LePage, P. Barboux, B. G. Bagley, L. H. Greene, W. R. McKinnon, G. W. Hull, M. Giroud, and D. M. Hwang, *Phys. Rev., B* **37,** 9382(1988).
11. J. M. Tarascon, W. R. McKinnon, P. Barboux, D. M. Hwang, B. G. Bagley, L. H. Greene, G. W. Hull, Y. LePage, N. Stoffel, and M. Giroud, *Phys. Rev., B* **38,** 8885 (1988).
12. J. L. Tallon, R. G. Buckley, P. W. Gilberd, M. R. Presland, I. W. M. Brown, M. E. Bowden, L. A. Christian, and R. Goguel, *Nature (London)* **333,** 153 (1988).
13. H. W. Zandbergen, P. Groen, G. Van Tendeloo, J. van Landuyt, and S. Amelinckx, *Solid State Commun.* **66,** 397 (1988).
14. C. C, Torardi, M. A. Subramanian, J. C. Calabrese, J. Gopalakrishnan, E. M. McCarron, K. J. Morrissey, T. R. Askew, R. B. Flippen, U. Chowdhry, and A. W. Sleight, *Phys. Rev., B* **38,** 225 (1988).

15. M. A. SUBRAMANIAN, C. C TORARDI, J. C. CALABRESE, J. GOPALAKRISHNAN, K. J. MORRISSEY, T. R. ASKEW, R. B. FLIPPEN, U. CHOWDHRY, AND A. W. SLEIGHT, *Science* **239,** 1015 (1988).
16. G. S. GRADER, E. M. GYORGY, P. K. GALLAGHER, H. M. O'BRYAN, D. W. JOHNSON, JR., S. SUNSHINE, S. M. ZAHURAK, S. JIN, AND R. C. SHERWOOD, *Phys. Rev., B* **38,** 757 (1988).
17. H.-X. ZHENG AND J. D. MACKENZIE, *Phys. Rev., B* **38,** 7166 (1988).
18. J. S. LUO, J.-P. CHEVALIER, AND D. MICHEL, *Mater. Sci. Eng. B* **3,** 325 (1989).
19. H. W. ZANDBERGEN, Y. K. HUANG, M. J. V. MENKEN, J. N. LI, K. KADOWAKI, A. A. MENOVSKY, G. VAN TENDELOO, AND S. AMELINCKX, *Nature (London)* **332,** 620 (1988).
20. J. M. TARASCON, Y. LEPAGE, L. H. GREENE, B. G. BAGLEY, P. BARBOUX, D. M. HWANG, G. W. HULL, W. R. MCKINNON, AND M. GIROUD, *Phys. Rev., B* 38, 2504 (1988).
21. Y. K. HUANG, K. KADOWAKI, M. J. V. MENKEN, J. N. LI, K. BAKKER, A. A. MENOVSKY, J. J. M. FRANSE, G. F. BASTIN, H. J. M. HEIJLIGERS, H. BARTEN, J. VAN DEN BERG, R. A. ZACHERN, AND H. W. ZANDBERGEN, *Physica C* **152,** 431 (1988).
22. K. NUMATA, K. MORI, H. YAMAMOTO, H. SEKINE, K. INOUE, AND H. MAEDA, *J. Appl. Phys.* **64,** 6392 (1988).
23. S. PEKKER, J. SASVARI, G. Y. HUTIRAY, AND L. MIHALY, *J. Less-Common Met.* **150,** 277 (1989).
24. Y. OKA, N. YAMAMOTO, H. KITAGUCHI, K. ODA, AND J. TAKADA, *Japan J. Appl. Phys. Lett.* **28,** L213 (1989).
25. H. NOBUMASA, K. SHIMIZU, Y. KITANO, AND T. KAWAI, *Japan J. Appl. Phys. Lett.* **27,** L846 (1989).
26. N. MURAYAMA, E. SUDO, M. AWANO, K. KANI, AND Y. TORII, *Japan J. Appl. Phys. Lett.* **27,** L1629 (1989).
27. J. S. LUO, D. MICHEL, AND J.-P. CHEVALIER, *Appl. Phys. Lett.* **55,** 1448 (1989).
28. S. KOYAMA, U. ENDO, AND T. KAWAI, *Japan J. Appl. Phys. Lett.* **27,** L1861 (1989).
29. T. HATANO, K. AOTA, S. IKEDA, K. NAKAMURA, AND K. OGAWA, *Japan J. Appl. Phys. Lett.* **27,** L2055 (1989).
30. NBS-ICTA standard reference material 760, NBS special publication 260-40, p. 57 (1971).
31. F. FAUDOT, M. HARMELIN, J. BIGOT, S. ARGOUIN, AND P. GOUÉROU, *Thermochim. Acta* **147,** 205 (1989).
32. IUPAC Recommendations, *Pure Appl. Chem.* **37,** 439 (1974).
33. M. HERVIEU, Communication at "Colloque Microstructure des Supraconducteurs à Haute Temperature Critique" Presqu'île de Giens, France, 1st to 3rd June, 1989.
34. M. HERVIEU, A. MAIGNAN, C. MARTIN, C. MICHEL, J. PROVOST, AND B. RAVEAU, *Mod. Phys. Lett. B* **2,** 1103 (1988).
35. C. N. R. RAO, R. VIJAYARAGHAVAN, L. GANAPATHI, AND S. V. BHAT, *J. Solid State Chem.* **79,** 177 (1989).
36. D. J. WERDER, C. H. CHEN, S. JIN, AND R. C. SHERWOOD, *J. Mater. Res.* **4,** 748 (1989).
37. R. RAMESH, C. J. D. HETHERINGTON, G. THOMAS, S. M. GREEN, C. JIANG, M. L. RUDEE, AND H. L. LUO, *Appl. Phys. Lett.* **53,** 615 (1988).
38. R. RAMESH, G. THOMAS, S. M. GREEN, Y. MEI, C. JIANG, AND H. L. LUO, *Appl. Phys. Lett.* **53,** 1759 (1988).
39. J. S. LUO, J.-P. CHEVALIER, AND D. MICHEL, *Rev. Phys. Appl.* **25,** 3 (1990).